Optical and Quantum Electronics (2024) 56:1195
https://doi.org/10.1007/s11082-024-06500-w

# Design of femtosecond microstructured poly lactic acid temporal scaffolds coated with hydroxyapatite by pulse laser deposition method for bone tissue regeneration

**L. Angelova[1] · A. Daskalova[1] · R. Mincheva[2] · E. Filipov[1] · A. Dikovska[1] · M. H. Fernandes[3,4] · S. Vig[3,4] · I. Buchvarov[5]**

Received: 29 September 2023 / Accepted: 30 January 2024 / Published online: 18 June 2024


**Abstract**
The aim of the present study is to create porous poly lactic acid (PLA)-based temporal cellular scaffolds with specifically designed topographical orientation by means of femtosecond laser (fs)-induced microstructuring, additionally functionalized by a nanometric layer of hydroxyapatite (HA) by the pulse laser deposition (PLD) method. For this purpose, surface micromodification of PLA samples by means of a CPA Ti:sapphire fs laser system ($\tau = 150$ fs, $\lambda = 800$ nm, $\nu = 0.5$ kHz), operating at fluence $F = 0.8$ J/cm$^2$ and scanning velocity $V = 3.8$ mm/s, was combined with PLD of thin layer of HA on the patterned PLA matrices for cellular scaffold surface additional nanofunctionalization. Each laser structured PLA scaffold was analyzed with respect to its control and laser processed surface, covered with HA. The multilevel structured scaffolds were investigated by SEM, EDX, 3D profilometer, AFM, micro-Raman and WCA analyses. Cytocompatibility studies with MG63 osteoblastic cells were also performed. Moreover, the cellular behavior was compared with the one observed on HA spin-coated fs microstructured PLA temporary scaffolds, in order to compare the two methods of functionalization. A disordered spreading on smooth surfaces to a tendency of cell orientation and elongation along the laser created grooves was monitored, along with increased alkaline phosphatase activity, which could essentially improve their subsequent practical application in engineering of personalized bone tissue.

**Keywords** Biopolymer cellular scaffolds · Femtosecond laser modification · Pulse laser deposition · Bone tissue engineering · Temporary cell matrices

✉ L. Angelova
liliya_angelova@ie.bas.bg; lily1986@abv.bg

[1] Institute of Electronics, Bulgarian Academy of Sciences, Sofia, Bulgaria

[2] Laboratory of Polymeric and Composite Materials (LPCM), University of Mons, Mons, Belgium

[3] LAQV/REQUIMTE, University of Porto, Porto, Portugal

[4] Faculdade de Medicina Dentaria, Universidade do Porto, Porto, Portugal

[5] Physics Department, Sofia University "St. Kliment Ohridski", Sofia, Bulgaria

## 1 Introduction

Temporary biocompatible and degradable cellular scaffolds, the modern tool of tissue regeneration and engineering in the face of personalized medicine, are emerging as one of the most powerful approaches for guided self-regeneration of damaged, fractured, or diseased bone tissues (Hutmacher et al. 2007; Scheinpflug et al. 2018; Bose et al. 2012). These structures serve as mechanically stable supporting platforms for the patient's own cell attachment and proliferation. They are gradually displaced by the newly formed tissue, resembling the remodeling of the natural bone in the case when this process could not be completed without the presence of a supportive component of the musculoskeletal system, for example, large scale bone fractures or injuries; osteoporosis or bone tumor resection (Datta et al. 2008; Scheinpflug et al. 2018; Wubneh et al. 2018). In this way, the natural regeneration could be completed without incorporating additional stress in the recipient, like permanent implants or donor shortage bone tissue, which might trigger an unintended immune response or inflammatory reaction (Olson et al. 2011; Bose et al. 2012).

In order to fulfil all "bone cellular demands" for effective regeneration of the connective tissue, the designed temporal scaffolds should possess qualitative and quantitative characteristics compatible with those of the extracellular matrix (ECM) of the bone tissue: a composite biocompatible, mechanically stable material of inorganic components (mainly in the form of calcium phosphates) and biodegradable organic (polymer-based) matrix, water, etc. (Clarke 2008; Scheinpflug et al. 2018). The aim of the present study is to design such a smart biomimetic extracellular scaffold in the form of hierarchically microstructured Poly-Lactic Acid temporal 2D matrix nanocoated with Hydroxyapatite by for bone tissue regeneration application. Poly-lactic acid (PLA) is a thermoplastic synthetic biodegradable polymer characterized by mechanical stability, plasticity, flexibility, elasticity, and strength (Rasal et al. 2010). It is approved by the Food and Drug Administration (FDA), as it can be excreted from the body by the natural catabolic pathways (Serra et al 2013; Hu et al. 2010), which has made PLA a basic matrix biomaterial in the design of temporal cell scaffolds (Santoro et al. 2016; Rasal et al. 2010). On the other hand, hydroxyapatite (HA) inorganic mineral crystals are the natural form in which calcium phosphates are found in the bone matrix (Wiesmann et al. 2005; Buckwalter et al. 1995). HA is responsible for the high mechanical stability and rigidity of the ECM of the bone, as well as the load-bearing properties of this connective tissue. Due to this mineral, a stable bond between the temporal scaffold and the surrounding bone tissue is made (Wang et al. 2013; Milella et al. 2001; Meskinfam et al. 2018), which makes it a perfect interface material for enhanced cellular adhesion.

PLA/Hydroxyapatite (HA) hybrid scaffolds are more similar to natural bone tissue in respect to elasticity, strength and mechanical compatibility than single mineral or polymer-based temporal scaffolds (Hu et al. 2010). For example, the group of Zhang et al., successfully fabricated a PLLA/nanohydroxyapatite composite and demonstrated that it has suitable compressive strength and good osteogenic properties (Zhang et al. 2021). The group of Castro et al. prepared biomimetic osteochondral scaffolds by integrating nanocrystalline hydroxyapatite and PLGA with hierarchical nano-to-micro structures, that showed improved human bone marrow-derived mesenchymal stem cell adhesion, proliferation, and osteochondral differentiation activity (Castro et al. 2015). On the other hand, Li and coworkers demonstrated specific myogenic differentiation of hMSCs, induced simply by ultra-fast laser generation of porous microchannels on a PLA-ε-caprolactone copolymer

cellular scaffold without the addition of any biological stimuli (Li et al. 2012). It has also been reported that the addition of HA to PLA scaffolds leads to enhanced adhesion, proliferation mineralization and expression of osteogenic genes by MC3T3-E1 osteoblastic cell line (Zhou et al. 2017). Further, in previous studies, we reported the development of biomimetic hierarchical structuring of PLA by ultra-short laser pulses (Daskalova et al. 2021) and also femtosecond laser followed by spin coating with chitosan or HA (Angelova et al. 2022).

The femtosecond laser technique, based on surface ablation of biocompatible materials, matrices and tissues, introduces controlled topographical features and multilevel micro/nanoporosity or roughness in a non-thermal and precisely controlled manner (Terakawa 2018). No unwanted side effects, damages, or changes in the chemical composition of the processed material are observed due to the ultra-fast nature of the interaction, while wettability, charge, roughness and porosity are finely tuned (Daskalova et al. 2019; Govindarajan et al. 2014). On the other hand, functionalization of the structured surfaces might be achieved by pulse laser deposition (PLD), entailing a high-power pulsed laser beam, focused inside a vacuum chamber to strike a target of the material that is to be deposited. This vaporized material, in the form of nanoparticle plasma, is deposited as a thin, nanometric film on the substrate (Surmenev 2012). Thus, for example, a previous study succeeded to deposit homogeneous crystalline hydroxyapatite thin coatings on silicon substrates by Nd:YAG (532 nm)-PLD at room temperature (Gomes et al. 2017). This process can occur in ultra-high vacuum or in the presence of a background gas, such as oxygen, which is commonly used when depositing oxides to fully oxygenate the deposited films. In their elaborate review Koch et al. describe in details the Pulsed laser deposition of hydroxyapatite thin films on different substrate materials for metallic orthopedic and dental prostheses (Koch et al. 2007). On the other hand, Terakawa revises the femtosecond laser processing of biodegradable polymers for biomedical application, including cell behavior control, tissue scaffolding, and drug release (Terakawa 2018). The innovative combining of the functionalization advantages of both methods, which is not known to have been performed until now, further enhances the advantages of each method. Moreover, such combination enables avoiding the drawbacks of conventional approaches (ex. solvent casting, gas foaming, phase separation, etc.) for the structuring of biomaterials, that in many cases could result in harmful chemical alternations, compromising the scaffolds' biocompatibility (O'Brien et al. 2015; Sears et al. 2016).

The aim of the present study is to create porous PLA-based temporary scaffolds with specifically designed topographical orientation by means of femtosecond laser-induced microstructuring, additionally functionalized with a thin layer of HA. Therefore, as a step forward, we propose a two levels scaffold functionalization in order to mimic the complex micro/nano-porous bone structure. In this way, hierarchical porosity, micro/nanoroughness and enchanted wettability could be achieved in a very controlled manner and cellular behaviour management could be further enhanced in respect to applying the two contactless methods separately. To accomplish this, PLA samples were surface-modified using a Chirp Pulse Amplification (CPA) Ti:sapphire fs laser system with previously optimized laser parameters (Angelova et al. 2022). Following that, a PLD approach was used to deposit a nanometric layer of HA on the patterned PLA matrices in order to functionalize the scaffold surface. In order to monitor their complementary impact on the PLA scaffolds properties, both surface laser structuring and PLD were applied to the 2D PLA samples. Each laser processed PLA scaffold was compared to its control and HA-functionalized laser processed surface. The multilevel structured scaffolds were investigated

by Scanning Electron Microscopy (SEM), Energy Dispersive X-ray elemental analysis (EDX), 3D profilometer, Atomic Force Microscopy (AFM), micro-Raman and Water Contact Angle (WCA) analyses. Cell viability studies with MG-63 osteoblastic cells were also performed. Moreover, the cellular behaviour was compared with that observed in seeded HA spin-coated fs microstructured PLA scaffolds previously developed and characterized (Angelova et al. 2022), in order to disclose the cellular response regarding the two methods of HA-nanofunctionalization. As a whole, disordered spreading on smooth surfaces with a tendency towards cell orientation and elongation along the laser created grooves was monitored. The results suggested that such combined methods find application for functionalization of the PLA scaffolds and can essentially improve the bioactivity properties of the microstructured PLA-hydroxyapatite nano designed hybrid matrices with potential application in the engineering of personalized bone tissue.

## 2 Materials and methods

The Carver 4122 12-12H Manual Heated Press (Carver Inc., USA) was used for the preparation of PLA plates with a thickness of around 220–250 μm and dimensions 1 × 1 cm. The raw PLA material (PLA 4060D, Nature Works, Nebraska, USA) was dried 12 h/60 °C under vacuum and molded according to the following compression molding procedure—3 min/180 °C, degassing cycles, 2 min/12 bars. The as prepared 2D PLA samples were ablated in air by means of a LabView-controlled Ti:Sapphire femtosecond laser system (Quantronix-Integra-C, Hamden, CT, USA), working in continuous mode of operation, at a central wavelength $\lambda = 800$ nm, $\tau = 150$ fs pulse duration, $\nu = 0.5$ kHz repetition rate, a fluence $F = 0.8$ J/cm$^2$ and a scanning velocity $V = 3.8$ mm/s. On the perpendicularly positioned on motorized XYZ translation stage samples, fs laser raster scanning was performed in the X–Z direction, as parallel microchannels with precisely defined porosity, dimensions, and distance between them were achieved on the surface. A nanometric layer of HA was deposited on the patterned PLA matrices by pulse laser deposition (PLD)—a standard ns-PLD configuration for thin film depositions. The films were fabricated by ablation of the HA target (LPCM, University of Mons, Belgium) with an Nd:YAG laser (Lotis LS-2147, pulse duration of 15 ns and 10 Hz repetition rate) working on its second harmonic wavelength at 532 nm. The laser fluence applied on the target was $F = 10$ J/cm$^2$. The target (HA)-substrate (PLA) distance was kept at 3 cm. All depositions were performed in vacuum (at pressure of $10^{-4}$ Torr) for a deposition time of 5 min. Each ablated PLA (fsPLA) surface was morphologically and chemically analyzed with respect to control (cPLA and cPLA-HA) and laser processed samples covered with HA (fsPLA-HA).

A Scanning Electron Microscope, SEM-TESCAN/LYRA/XMU (TESCAN ORSAY HOLDING, a.s., Brno, Czech Republic), equipped with an Energy Dispersive X-ray module (EDX Quantax 200, Bruker), working at an operational voltage of 10 kV, was used for surface morphology and elemental composition evaluation. The samples were carbon covered by a sputtering system (Quorum Technologies) under vacuum. SEM images were taken at 1.5kx magnification, and the corresponding elemental composition [wt%] was also defined. The surface roughness of the PLA plates was characterized via 3D Optical profiler, Zeta-20. The roughness parameters Ra and Sa were measured by means of line and area roughness analysis as an average value over five separate measurements (ISO 4287).

ProfilmOnline software (https://www.profilmonline.com) was used for better visualization of the 3D profile of the laser scan pattern in the obtained true colour images. The width and depth of the laser created grooves were also evaluated. An atomic force microscope, MultiMode V (Veeco Instruments Inc., New York, NY, USA), equipped with controller, NanoScope V (Bruker Ltd., Berlin, Germany), was used in order to obtain 2D and 3D images over an area of 15 × 15 μm and 5 × 5 μm. For this purpose, a Tap150Al-G (BudgetSensors, Switzerland) silicon AFM probe in dynamic tapping mode of operation was applied for nanosurface area (Sa) roughness evaluation. A microRaman spectrometer (LabRAM HR Visible, HORIBA Jobin Yvon, Kyoto, Japan), equipped with Olympus BX41 microscope and working with a He–Ne laser (632 nm), was used for obtaining the micro-Raman profile of the samples investigated (time of exposition-20 s at 50 × magnification). Dynamic Water Contact Angle (WCA) measurements for a period of 180 s and an average $dH_2O$ volume of 2 μl of 2D PLA plates before and after laser structuring and HA-deposition were performed in air by a video-based optical contact angle measurement device, the DSA25 Drop Shape Analyzer (KRÜSS GmbH). Contact angles were calculated by ADVANCE software (KRÜSS GmbH) by fitting the drop profiles to the Young–Laplace equation. Each value was averaged over five separate measurements. In vitro biological evaluation of the examined 2D PLA plates with MG-63 osteoblastic cell line (ATCC®CRL-1427™) was also performed. The cellular behaviour was compared with the one observed on seeded Hydroxyapatite spin-coated fs microstructured PLA temporary scaffolds (Angelova et al. 2022). The osteoblast-like MG63 cells were cultured in alpha-MEM medium supplemented with 10% fetal bovine serum (FBS), 100 IU/mL penicillin, 100 μg/mL streptomycin, and 2.5 μg/mL amphotericin B (all reagents from Gibco, USA) at 37 °C, 95% humidity and 5% $CO_2$/air atmosphere for cytocompatibility assessment. Cells were seeded over the material samples at a density of $4 \times 10^4$ cells/$cm^2$ and cultured for a period of 10 days, in the absence of osteogenic factors. Cell response was evaluated for metabolic activity/proliferation (days 2, 5 and 10; Resazurin assay), alkaline phosphatase (ALP) activity (day 10) and SEM and fluorescence imaging (day 5). On the Resazurin assay, seeded materials were incubated in a 10% Resazurin solution (Resazurin sodium salt, Sigma-Aldrich R7017) prepared in complete alpha-MEM medium (as described above) for 3 h at 37 °C. The fluorescence signal (530 nm excitation/590 nm emission) was evaluated in a microplate reader (Synergy HT, Biotek, Winooski, VT, USA) with Gen5 1.09 Data Analysis Software. ALP was assessed in cell lysates prepared in 0.1% Triton X-100 for a period of 30 min, by the hydrolysis of p-nitrophenyl phosphate substrate (p-NPP, 25 mM, Sigma-Aldrich, USA) in an alkaline buffer (pH 10.3, 37 °C, 1 h). NaOH (5 M) was used to stop the reaction, and p-nitrophenol (the reaction product) was measured at 400 nm in a microplate reader (Synergy HT, Biotek, USA). The results were normalized to total protein content, measured according to the manufacturer's instructions by DCTM Protein Assay (BioRad, Hercules, CA, USA), and presented as nanomoles of p-nitrophenol per microgram of protein (nmol/μg protein). For SEM observation, cells were fixed, dehydrated in graded alcohol, critical point dried, and sputter coated with a palladium/gold alloy prior to imaging (FEI Quanta 400 FEG/ESEM). Fluorescence imaging (Celena S digital imaging system, Logos Biosystems, Anyang, South Korea) was performed in fixed samples stained for F-actin cytoskeleton (Alexa Fluor® 488 phalloidin; 1:100, 30 min; Molecular Probes, Eugene, OR, USA), and nucleus with Hoechst (8 μg/mL, 10 min, Enzo, NY, USA).

## 3 Results and discussion

### 3.1 Morphological analysis of 2D PLA scaffolds-SEM micro and AFM nano roughness analysis

The multicomponent Fig. 1 represents a compilation of the following results (from left to right): SEM images, taken at 1500 × magnification, the corresponding 2D, 3D true colour microroughness images and Ra-line roughness cross-section profiles of the fsPLA-HA (laser structured PLA sample, PLD-covered with nanolayer of HA) Fig. 1a, fsPLA (laser structured PLA) Fig. 1b, cPLA-HA (control PLA, PLD-covered with HA) Fig. 1c and cPLA (control PLA) Fig. 1d). As can be easily seen from the SEM and 3D profilometer images, the porous laser-generated channels on the surface of fsPLA samples (Fig. 1a, b) are clearly outlined with defined dimensions and reproducible pattern with respect to the visibly smooth surface of the control plates (Fig. 1c, d); no mechanical damage to the material is detected. Moreover, when sputtered with HA, no morphological difference at microlevel was observed with respect to the corresponding control sample—the depth and width of the laser micro-channels remained in the same order of magnitude—their overall dimensions decreased with approximately 30 nm, which could be attributed to the pulse laser deposited HA "layer". At the same time, no change in the cross-section profile of the

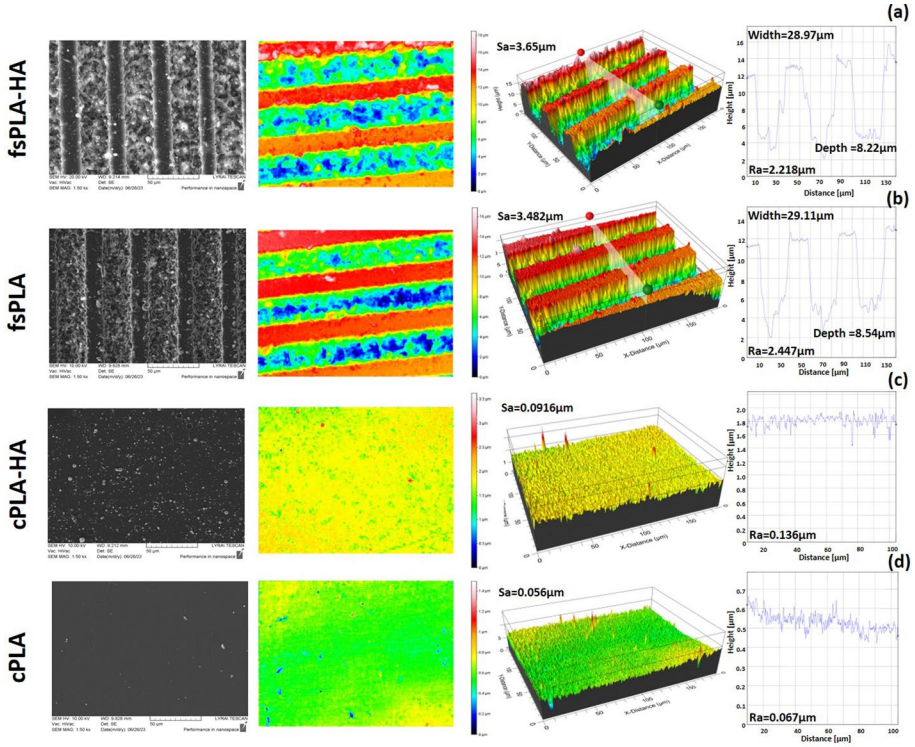


**Fig. 1** A multicomponent image, representing a compilation of the SEM images (1500 × magnification) and the corresponding 2D, 3D true colour microroughness images and Ra-line roughness cross-section profiles of: **a** fsPLA-HA; **b** fsPLA; **c** cPLA-HA and **d** cPLA

fs laser processed PLA plates is observed. The HA deposition does not disturb the surface pattern created by the laser (Fig. 1a, b)—on the one hand, the clean U-shaped edges of the grooves, are clearly distinguishable, while, at the same time, the nano-HA layer applied could lead to additional surface functionalization and subsequent cellular adhesion and differentiation, in line with previous results (Daskalova et al. 2021; Angelova et al. 2022). This is due to the osteoconductive properties (Wiesmann et al. 2005) and high "bonding" capacity of HA with surrounding bone tissue (Milella et al. 2001). The values of Sa and Ra parameters, also given on Fig. 1 confirm these results—after laser treatment, the surface roughness (Sa) increases 4 times—from 92 nm up to 3.65 µm; the Sa values are in the same order after PLD with HA, of course, taking into account the 30 nm layer of the ceramic material deposited on top of the cPLA and fsPLA (Fig. 1—last column). The Ra values, on the other hand, stay under 2.5 µm, which falls into the optimal range for stable bond formation of the temporal scaffold surface to recipient tissue (Riveiro et al. 2012; Ponsonnet et al. 2003) and on the other hand, could help cellular focal contact formation and adhesion (Bacáková et al. 2004; Szmukler et al. 2004). According to literature, the optimum roughness Ra value is higher than = 1 µm (Ponsonnet et al. 2003). This fact was also confirmed by our research group, which has previously reported enhanced MSCs adhesion and orientation along with the laser generated porous structures on PLA surface (Daskalova et al. 2021).

The results of the performed AFM analysis (Fig. 2) supplement the presented surface morphology data. HA does not form a continuous nanolayer on the surface of the PLA scaffolds. During the PLD process, the interaction of the Nd:YAG laser beam with the HA tablet leads to the formation of a cloud of ablated HA particles in the vacuum chamber, and part of these nanoparticles are deposited on the sample surface, thus a nanometric roughness is achieved (Fig. 2). As can be easily seen from the AFM images (Fig. 2-nano level) and SEM images (Fig. 1-micro level), the HA nanoparticles (with an average diameter in the range of 2 ÷ 5 nm up to 10 ÷ 12 nm) add characteristic nanoroughness, both on the control and laser microstructured PLA samples. The Sa values inside the laser grooves and on the surface of the control samples increased after the pulse laser deposition of HA has been

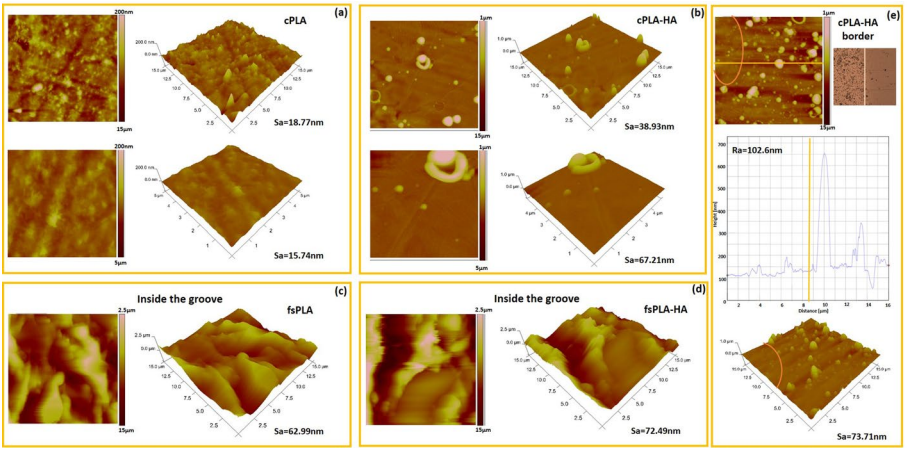


**Fig. 2** Representative selection of 2D and 3D AFM images at 15×15 µm and 5×5 µm of: **a** cPLA, **b** cPLA-HA and inside the fs-grooves of **c** fsPLA and **d** fsPLA-HA; **e** cPLA-HA border-optical (50×), 2D/3D AFM images and the Ra-line roughness cross-section profile

performed (Fig. 2). Clusters of HA particles with specific forms and dimensions up to several hundred nm are also observed, rather like an exception to the general HA background. The border between the deposited HA and control zones is easily distinguishable on the optical, 2D/3D AFM images and the Ra-line roughness cross-section profile, presented on the rightmost part of the Fig. 2. These results comply with those found in the literature. The group of Majhy et al., for example, reported optimal intermediate nanoroughness in the range of 5–150 nm as providing the most favourable conditions for efficient cell adhesion, growth, and proliferation (Majhy et al. 2021).

### 3.2 EDX, micro-Raman analysis and WCA evaluation of the examined PLA samples

The results of the performed EDX analysis are presented in Fig. 3 (left) in the form of EDX spectra with the corresponding—EDX [wt%] elemental concentration. All elements of interest, C, O; Ca, and P (for HA functionalized samples), are detected by the EDX analysis. At the same time, no peaks of uncommon elements are observed in the spectra. The detection of lower values of C [wt%] and higher values of O [wt%] concentration, after ablation in respect to the control surface of the corresponding sample (cPLA, cPLA-HA) could be explained by the breakage of side O–C=O chemical bonds from the PLA backbone leading to surface oxidation, attributed to the fs laser interaction with the polymer material, as it has already been reported by our group (Angelova et al. 2022). The Ca and P elements were detected only in the HA nanofunctionalized PLA scaffolds. But when comparing the elemental composition of the HA laser deposited PLA matrices (cPLA-HA and fsPLA-HA), the preferential accumulation of HA on the fs structured surface is clearly distinguished. An increase of almost 6 times higher concentration of [wt%] of Ca and P on laser modified PLA was monitored, in respect to the control surface. The results comply with previously published ones, obtained after nanofunctionalization of the fs structured 2D PLA scaffolds by the method of spin-coating, where the hydroxyapatite accumulated up to 5–7 times higher on the structures, created by the laser processing (Angelova et al. 2022).

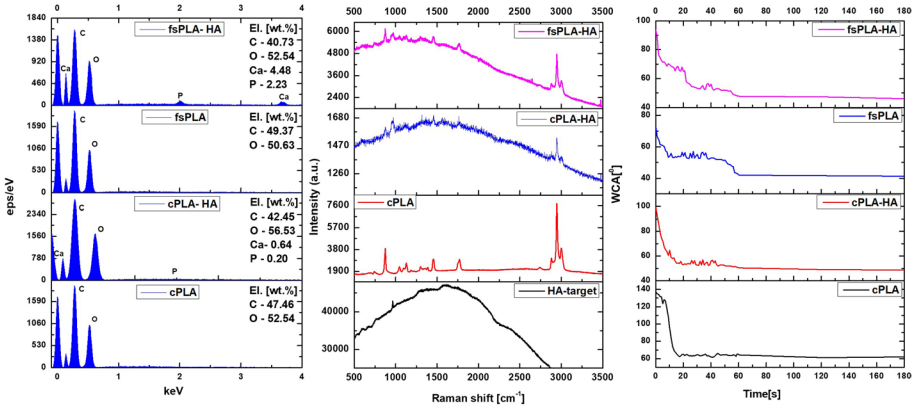


**Fig. 3** EDX spectra with corresponding [wt%] elemental concentration (left) and dynamic WCA measurement for a period of 3 min (right) of: cPLA, cPLA-HA, fsPLA, fsPLA-HA; micro-Raman spectra (middle) of HA-target, cPLA, cPLA-HA and fsPLA-HA

The presence of HA in the nanofunctionalized PLA samples was also observed using Raman spectroscopy—Fig. 3 (middle) where the microRaman spectra for cPLA-HA and the fsPLA-HA composite plates are presented. All characteristic bands of PLA are observed as follows: picks at 2997 $cm^{-1}$, 2990 $cm^{-1}$, and 2876 $cm^{-1}$—attributed to asymmetric and symmetrical stretching vibrations of the C–H bond of the PLA molecule backbone; 1760 $cm^{-1}$—stretching vibration of the C=O bond; 1451 $cm^{-1}$—the asymmetric deformation vibration of the $CH_3$ bond and 885 $cm^{-1}$, which is due to the stretching vibration of the C–COO bond (Gong et al. 2017). The presence of the inorganic HA in the PLD nano-covered samples is clearly evidenced by the presence of an additional band around 961 $cm^{-1}$ which corresponds to the $PO_4^{3-}$ stretching vibration (Cukrowski et al. 2007). The intensity of this peak is higher for fsPLA-HA samples in respect to the corresponding control, which correlates with the results obtained from the EDX analysis performed Fig. 3 (left). The microRaman spectra of the HA tablet, used as a PLD target and of cPLA are also given as a reference.

The WCA measurements Fig. 3 (right), were performed for a period of 180 s in parallel direction to the laser-generated microchannels (for the fsPLA and fsPLA-HA). As can be seen from the 4 graphs presented, the laser structured surfaces and the HA-sputtered ones are more hydrophilic than the corresponding controls, making the substrate "cell adhesive friendly", which could improve the biocompatibility of the PLA temporal scaffolds (Gittens et al. 2014).

For example, Wan et al., report a WCA (θ) of 20°–55° as optimal for endothelial cell adhesion and expansion on porous poly-(L-lactide) surfaces (Wan et al. 2003). This corresponds to the case of fsPLA and fsPLA-HA, with mean WCA values 47.2° and 41.1°, respectively. By increasing the contact time of the water drop with the PLA scaffolds surface, due to surface wetting, a general trend of lowering the water contact angle values is observed for the four groups of 2D PLA scaffolds. After around 60 s, WCA stabilizes, but during this period fluctuations in the lowering values of WCA are observed, especially for the fs laser structured samples. These "up and down jumps" in the values could be explained by the heterogeneous wetting model, established by Cassie and Baxter (Cassie et Baxter 1944). The formation of the periodical laser-structured microchannels on the PLA scaffold (fsPLA and fsPLA-HA), leads to air pockets accumulation in the volume of the hierarchically porous structure (a solid–liquid–air interface is formed). This leads to the initial non-uniform expansion of the water droplet inside the laser created microstructure, and subsequently, results in sudden twists in the WCA values which form the uneven appearance of the graph during the first 60 s of water droplet application—Fig. 3 (right)—fsPLA and fsPLA-HA. These results supplement the ones obtained after morphological evaluation of the PLA temporal scaffolds (Figs. 1 and 2). The nanoroughness added by the accumulation of HA particles on the PLA surface is also reflected in the graph's appearance in the form of lower (cPLA-HA), superimposed (on the miccrostrucrured fsPLA-HA) fluctuations in the WCA values during first minute. In any case, the HA-functionalization leads to 10° drop in the mean value of WCA on 3rd minute of drop application, after reaching equilibrium (cPLA—60.3° to 49.8° for cPLA-HA). This leads to a more hydrophilic, cellular focal contact formation- and adhesion-promoting surface (Bacáková et al. 2004). The enhanced surface wettability and surface roughness, both in the optimal range for efficient cell adhesion, growth, and proliferation (Majhy et al. 2021; Wan et al. 2003) in combination with no elemental composition alterations, and the enhanced bonding capacity of the HA-functionalized micro structured porous PLA temporal implant surface to the recipient own bone tissue could eventually lead to successful application for bone implant in vivo regeneration.

### 3.3 Osteoblastic cell response on PLD HA-functionalized fs structured PLA scaffolds

MG63 osteoblastic cells were cultured over PLD HA-functionalized fs structured PLA scaffolds for 10 days, and cell response was evaluated for morphology and pattern of cell growth, viability/proliferation and ALP activity, as summarized in Fig. 4a (left panel). In order to evaluate and compare two methods of surface nano-functionalization in the form of nano-HA particles or layer (PLD and spin-coating, respectively) of the fs processed PLA scaffolds, cellular behaviour on HA spin-coated fs microstructured PLA scaffolds was also performed in parallel using the same experimental setup (Fig. 4b—right panel). Morphological and chemical evaluation of the spin-coated scaffolds (structured in similar conditions, with the same laser parameters) were previously published by our research group (Angelova et al. 2022). In brief, the combined application of fs laser structuring with the precise spin-coating method for surface functionalization of PLA scaffolds leads to improved wettability, laser-enhanced surface roughness and porosity, no chemical structure alterations, and to several times improved deposition of HA on ultra-fast laser-processed areas (Angelova et al. 2022); the main difference with the scaffolds presented in the current study is expressed in the form of the HA deposition—continuous nanometric layer in the case of spin-coating and surface material deposition in the form of nanoparticles, when PLD is used for functionalization.

SEM and fluorescence imaging of the seeded materials showed that the general trend observed on the two types of functionalized samples is a disordered cell spreading and random distribution on the smooth surfaces (not laser structured) as evident in Fig. 4a-A, B, and a clear trend of cell orientation and elongation along the laser created grooves (Fig. 4a-A, B, b-B). These observations correlate with the results obtained by Daskalova et al. (2021) who demonstrated experimentally the orientation of Wharton Jelly Mesenchymal

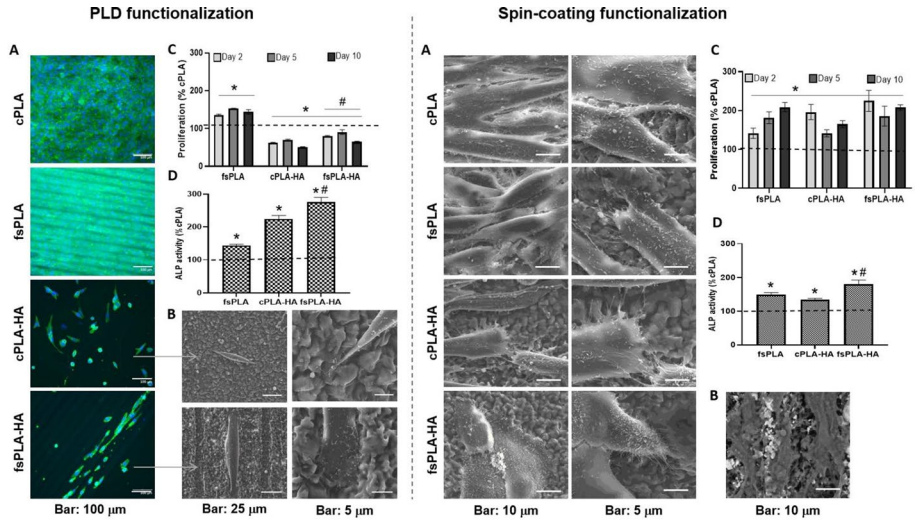


**Fig. 4** Behaviour of osteoblastic cells cultured over fs laser-structured PLA scaffolds further functionalized with HA by PLD (**a**—left panel) or spin-coating (**b**—right panel). Material samples were cultured for 10 days and evaluated for SEM and fluorescence imaging (at day 5), cell viability/proliferation (at days 2, 5 and 10) and alkaline phosphatase (ALP) activity (at day 10). Quantitative results are presented as % of control (cPLA). *Significantly different from control ($p \leq 0.05$); #Significantly different from fsPLA ($p \leq 0.05$)

Stem Cells (MSCs) on fs structured PLA samples. The group of Cordero et al. for example, showed better arrangement of MC3T3-E1 pre-osteoblastic cells on laser microstructures (Cordero et al. 2013) and on the other hand Zhou and coworkers reported that the addition of HA to PLA scaffolds leads to enhanced adhesion, proliferation mineralization and expression of osteogenic genes by MC3T3-E1 osteoblastic cell line. Moreover, they reported that the cells stretched better on the PLLA/HA scaffolds than the control group at day 7 and that the such hybrid scaffolds were more favorable for bone cell adhesion (Zhou et al. 2017). Nevertheless, in our study, all scaffolds allowed cytoplasmic spreading with abundant extensions and established cell-to-cell and cell materials interactions. Results for viability/proliferation showed increased values on the laser structured surfaces (fsPLA) compared to the control (cPLA), Fig. 4a-C and Fig. 4b-C. Also, HA spin-coated samples (cPLA-HA and fsPLA-HA) allowed a significantly higher proliferation compared to cPLA (Fig. 4b-C). However, on PLD HA-functionalized scaffolds, cell proliferation was lower than that observed on cPLA and fsPLA (Fig. 4a-C). This is probably attributed to the deposition method (PLD or spin-coating), rather than the laser structuring itself (as the same laser parameters were used in the two scaffold types). This might be related with a higher initial burst of ions' release from the PLD functionalized scaffolds impairing the cell adhesion process, thus explaining the lower proliferation values compared to the HA spin-coated materials. The detected amorphous structure of HA nanoparticles deposited by PLD (XRD performed, not included in the manuscript) could contribute to the suggested initial ion release. Results for ALP activity, an established osteogenic marker, (Fig. 4a-D and Fig. 4b-D) showed increased values for the fs structured surfaces without and with HA functionalization, compared to cPLA. Interestingly, ALP activity was highest on the PLD functionalized samples (Fig. 4a-D) compared to the spin-coated ones (Fig. 4b-D). Considering the known inverse relationship between proliferation and osteoblastic differentiation, the results observed in the samples functionalized by PLD (decreased proliferation and higher ALP activity) might suggest a higher differentiation of the cells at this time point. Overall, compared to cPLA, the treated matrices showed the same trend of osteogenic behaviour, i.e. an increased differentiation on the fs laser-structured samples that was further enhanced by HA functionalization.

## 4 Conclusion

In the current study, an innovative combination of contactless, highly precise, and reproducible laser methods for surface micro/nano functionalization of temporal bone scaffolds was proposed. The presented experimental results clearly show that the combined application of fs laser microstructuring with the precise PLD HA-surface nano-deposition leads to improved wettability, laser-enhanced surface roughness and porosity, without elemental composition alterations of the investigated PLA matrices, and even to several times improved deposition of HA on ultra-fast laser-processed samples. Moreover, the HA nanoparticle deposition does not disturb the surface porous morphology, generated due to the ultra-fast processing—the width and depth of the laser-generated grooves are kept within the same microrange (suitable for MG63 osteoblastic cells seeding), without observing fluctuations in their cross-sectional transverse profile. The subsequent impact of both surface modification methods was monitored in order optimized scaffold properties to be achieved. Behaviour of osteoblastic cells seeded on these samples was compared to that observed on HA spin-coated fs microstructured PLA scaffolds, in order to compare

the two HA-functionalization procedures. Disordered spreading on control surfaces to cellular orientation and elongation along the laser created grooves was observed. All matrices allowed both cell-to-cell and cell-to-scaffold interactions. Despite some differences on cell proliferation, the two HA deposition methods yielded a similar cellular behaviour regarding ALP activity, namely an increased osteoblastic differentiation on the fs laser-structured samples that was further enhanced by HA functionalization. Comparatively, the data obtained suggested that PLD nano-functionalization with HA resulted in additional cellular differentiation.

The results obtained show that after PLD additional parameters optimization (as a next step in our studies), such combined methods could find application for functionalization of the bone PLA scaffolds. Such combination can essentially improve the bioactivity properties of the as created microstructured PLA-hydroxyapatite nanodesigned hybrid cell matrices and their subsequent practical application in engineering of personalized bone tissue, by enhancing the interface contact of the temporal scaffolds and the patient own tissues and promoting the acceptance of the implant by the body. This is due to the enhanced hierarchical microporosity of the PLA introduced by fs structuring, which is a prerequisite for the penetration of the cells into the depth of the created 3D porous network and the nano-HA, deposited by PLD on the other hand, that is the basis for a stable bond between the temporal scaffold and the surrounding bone. The enhanced surface wettability and surface roughness, both in the optimal diapason for efficient cell adhesion, growth, and proliferation in combination with no elemental composition alterations, and the enhanced bonding capacity of the HA-functionalized microstructured porous PLA temporal implant surface to recipient own bone tissue could eventually lead to successful application for bone implant in vivo regeneration.

**Acknowledgements** This research was funded by BULGARIAN NATIONAL SCIENCE FUND (NSF) under grant number No. KP-06-H48/6 (2020–2023), "Development of hybrid functional micro/nanoporous biomaterial scaffolds by ultra-fast laser modification", EUROPEAN UNION'S H2020 research and innovation programme under the Marie Sklodowska-Curie Grant Agreement No. 861138, and H2020 FET Open METAFAST Grant Agreement No. 899673.

**Author contributions** Conceptualization, L.A., A.D.; methodology, L.A., A.D.; writing, L.A., A.D., M.H.F.; original draft preparation, L.A.; project administration, A.D.; writing, L.A.; investigation, L.A., E.F, S.V., R.M., A.D.; visualization, L.A., S.V.; supervision, A.D, M.H.F., I.B. All authors reviewed the manuscript. All authors have read and agreed to the published version of the manuscript.

## Declarations

**Conflict of interest** The authors have no relevant financial or non-financial interests to disclose.

## References

Angelova, L., Daskalova, A., Filipov, E., et al.: Analysis of femtosecond microstructured poly lactic acid temporary cell scaffolds, spin-coated with chitosan or hydroxyapatite. Opt. Quant. Electron. **54**, 721 (2022)

Bacáková, L., Filová, E., Rypácek, F., Svorcík, V., Starý, V.: Cell adhesion on artificial materials for tissue engineering. Physiol. Res. **53**(Suppl. 1), S35–S45 (2004)

Bose, S., Roy, M., Bandyopadhyay, A.: Recent advances in bone tissue engineering scaffolds. Trends Biotechnol. **30**, 546–554 (2012)

Buckwalter, J.A., Glimcher, M.J., Cooper, R.R., Recker, R.: Bone biology. Part 1: structure, blood-supply, cells, matrix and mineralization. J. Bone Jt. Surg. Am. **77**, 1256–1275 (1995)

Cassie, A.B.D., Baxter, S.: Wettability of porous surfaces. Trans. Faraday Soc. **40**, 546–551 (1944)

Castro, N.J., O'Brien, J., Zhang, L.G.: Integrating biologically inspired nanomaterials and table-top stereolithography for 3D printed biomimetic osteochondral scaffolds. Nanoscale **7**, 14010–14022 (2015)
Clarke, B.: Normal bone anatomy and physiology. Clin. J. Am. Soc. Nephrol. **3**, S131–S139 (2008)
Cordero, D., López-Álvarez, M., Rodríguez-Valencia, C., Serra, J., Chiussi, S., González, P.: In vitro response of pre-osteoblastic cells to laser microgrooved PEEK. Biomed. Mater. **8**, 055006 (2013)
Cukrowski, I., Popovic, L., Barnard, W., Paul, S.O., van Rooyen, P.H., Liles, D.C.: Modeling and spectroscopic studies of bisphosphonate–bone interactions. The Raman, NMR and crystallographic investigations of Ca–HEDP complexes. Bone **41**, 668–678 (2007)
Daskalova, A., Bliznakova, I., Angelova, L., Trifonov, A., Declercq, H., Buchvarov, I.: Femtosecond laser fabrication of engineered functional surfaces based on biodegradable polymer and biopolymer/ceramic composite thin films. Polymers **11**, 378 (2019)
Daskalova, A., Angelova, L., Filipov, E., Aceti, D., Mincheva, R., Carrete, X., Kerdjoudj, H., Dubus, M., Chevrier, J., Trifonov, A., Buchvarov, I.: Biomimetic hierarchical structuring of PLA by ultra-short laser pulses for processing of tissue engineered matrices: study of cellular and antibacterial behavior. Polymers **13**, 2577 (2021)
Datta, H.K., Ng, W.F., Walker, J.A., Tuck, S.P., Varanasi, S.S.: The cell biology of bone metabolism. J. Clin. Pathol. **61**, 577–587 (2008)
Gittens, R.A., Olivares-Navarrete, R., Schwartz, Z., Boyan, B.D.: Implant osseointegration and the role of microroughness and nanostructures: lessons for spine implants. Acta Biomater. **10**, 3363–3371 (2014)
Gomes, G.C., Borghi, F.F., Ospina, R.O., López, E.O., Borges, F.O., Mello, A.: Nd:YAG (532 nm) pulsed laser deposition produces crystalline hydroxyapatite thin coatings at room temperature. Surf. Coat. Technol. **329**, 174–183 (2017)
Gong, M., Zhao, Q., Dai, L., Li, Y., Jiang, T.: Fabrication of polylactic acid/hydroxyapatite/graphene oxide composite and their thermal stability, hydrophobic and mechanical properties. J. Asian Ceram. Soc. **5**, 160–168 (2017)
Govindarajan, T., Shandas, R.: A survey of surface modification techniques for next-generation shape memory polymer stent devices. Polymers **6**, 2309–2331 (2014)
Hu, J., Sun, X., Ma, H., Xie, Ch., Chen, Y.E., Ma, P.X.: Porous nanofibrous PLLA scaffolds for vascular tissue engineering. Biomaterials **31**, 7971–7977 (2010)
Hutmacher, D.W., Schantz, J.T., Lam, C.X.F., Tan, K.C., Lim, T.C.: State of the art and future directions of scaffold-based bone engineering from a biomaterials perspective. J. Tissue Eng. Regener. Med. **1**, 245–260 (2007)
Koch, C.F., Johnson, S., Kumar, D., Jelinek, M., Chrisey, D.B., Doraiswamy, A., Jin, C., Narayan, R.J., Mihailescu, I.N.: Pulsed laser deposition of hydroxyapatite thin films. Mater. Sci. Eng. C **27**, 484–494 (2007)
Li, H., Wen, F., Wong, Y.S., Boey, F.Y., Subbu, V.S., Leong, D.T., Ng, K.W., Ng, G.K., Tan, L.P.: Direct laser machining-induced topographic pattern promotes up-regulation of myogenic markers in human mesenchymal stem cells. Acta Biomater. **8**, 531–539 (2012)
Majhy, B., Priyadarshinia, P., Sen, A.K.: Effect of surface energy and roughness on cell adhesion and growth—facile surface modification for enhanced cell culture. RSC Adv. **11**, 15467–15476 (2021)
Meskinfam, M., Bertoldi, S., Albanese, N., Cerri, A., Tanzi, M.C., Imani, R., Baheiraei, N., Farokhi, M., Fare, S.: Polyurethane foam/nano hydroxyapatite composite as a suitable scaffold for bone tissue regeneration. Mater. Sci. Eng. C Mater. Biol. Appl. **82**, 130–140 (2018)
Milella, E., Cosentino, F., Licciulli, A., Massaro, C.: Preparation and characterization of titania/hydroxyapatite composite coatings obtained by sol–gel process. Biomaterials **22**, 1425–1431 (2001)
O'Brien, C., Holmes, B., Faucettm, S., Zhang, L.G.: 3D printing of nanomaterial scaffolds for complex tissue regeneration. Tissue Eng. B Rev. **21**, 1–45 (2015)
Olson, J., Atala, A., Yoo, J.: Tissue engineering: current strategies and future directions. Chonn. Med. J. **47**, 1–13 (2011)
Ponsonnet, L., Reybier, K., Jaffrezic, N., Comte, V., Lagneau, C., Lissac, M., Martelet, C.: Relationship between surface properties (roughness, wettability) of titanium and titanium alloys and cell behavior. Mater. Sci. Eng. C **23**, 551–560 (2003)
Rasal, R.M., Hirt, D.E.: Poly(lactic acid) toughening with a better balance of properties. Macromol. Mater. Eng. **295**, 204–209 (2010)
Riveiro, A., Soto, R., Comesaña, R., Boutinguiza, M., Del Val, J., Quintero, F., Lusquiños, F., Pou, J.: Laser surface modification of PEEK. Appl. Surf. Sci. **258**, 9437–9442 (2012)
Santoro, M., Shah, S.R., Walker, J.L., Mikos, A.G.: Poly(lactic acid) nanofibrous scaffolds for tissue engineering. Adv. Drug Deliv. Rev. **107**, 206–212 (2016)
Scheinpflug, J., Pfeiffenberger, M., Damerau, A., Schwarz, F., Textor, M., Lang, A., Schulze, F.: Journey into bone models: a review. Genes **9**, 247–283 (2018)

Sears, N.A., Seshadri, D.R., Dhavalikar, P.S., Cosgriff-Hernandez, E.: A review of three-dimensional printing in tissue engineering. Tissue Eng. B Rev. **22**, 298–310 (2016)
Serra, T., Mateos-Timoneda, M.A., Planell, J.A., Navarro, M.: 3D printed PLA-based scaffolds. Organogenesis **9**, 239–244 (2013)
Surmenev, R.A.: A review of plasma-assisted methods for calcium phosphate-based coatings fabrication. Surf. Coat. Technol. **206**, 2035–2056 (2012)
Szmukler-Moncler, S., Perrin, D., Ahossi, V., Magnin, G., Bernard, J.P.: Biological properties of acid etched titanium implants: effect of sandblasting on bone anchorage. J. Biomed. Mater. Res. B Appl. Biomater. **68**, 149–159 (2004)
Terakawa, M.: Femtosecond laser processing of biodegradable polymers. Appl. Sci. **8**, 1123 (2018)
Wan, Y., Yang, J., Yang, J., Bei, J., Wang, S.: Cell adhesion on gaseous plasma modified poly-(L-lactide) surface under shear stress field. Biomaterials **24**, 3757–3764 (2003)
Wang, D.X., He, Y., Bi, L., Qu, Z.H., Zou, J.W., Pan, Z., Fan, J.J., Chen, L., Dong, X., Liu, X.N., et al.: Enhancing the bioactivity of poly(lactic-co-glycolic acid) scaffold with a nano-hydroxyapatite coating for the treatment of segmental bone defect in a rabbit model. Int. J. Nanomed. **8**, 1855–1865 (2013)
Wiesmann, H.P., Meyer, U., Plate, U., Hohling, H.J.: Aspects of collagen mineralization in hard tissue formation. Int. Rev. Cytol. **242**, 121–156 (2005)
Wubneh, A., Tsekoura, E.K., Ayranci, C., Uludag, H.: Current state of fabrication technologies and materials for bone tissue engineering. Acta Biomater. **80**, 1–30 (2018)
Zhang, B., Wang, L., Song, P., Pei, X., Sun, H., Wu, L., Zhou, Ch., Wang, K., Fan, Y., Zhang, X.: 3D printed bone tissue regenerative PLA/HA scaffolds with comprehensive performance optimizations. Mater. Des. **201**, 109490 (2021)
Zhou, G., Liu, S., Ma, Y., Xu, W., Meng, W., Lin, X., Wang, W., Wang, S., Zhang, J.: Innovative biodegradable poly(L-lactide)/collagen/hydroxyapatite composite fibrous scaffolds promote osteoblastic proliferation and differentiation. Int. J. Nanomed. **12**, 7577–7588 (2017)